Communication in Physical Sciences, 2024, 10(3): 239-249

Synthesis and Characterization of Calcium Oxide Nanoparticles (CaO-NPs) from Waste Oyster Shells

Richard Alexis Ukpe

Received: 04 March 2023/Accepted: 17 January 2024/Published: 29 January 2024

Abstract: *This study describes a method for synthesizing calcium oxide nanoparticles (CaO-NPs) from oyster shells, a waste material. The characterization of the synthesized CaO-NPs was conducted using X-ray diffraction (XRD), UV-visible spectroscopy, Raman spectroscopy, Fourier Transform Infrared (FTIR) spectroscopy, and dynamic light scattering (DLS). The XRD analysis confirmed the formation of CaO-NPs with an average crystal size of 57.18 nm. The UV-visible spectrum revealed maximum absorption at 206 nm, indicating absorption in the ultraviolet region. The band gap energy of the CaO-NPs, determined using the Tauc plot, was found to be 5.90 eV and 5.93 eV for direct allowed and indirect forbidden transitions, respectively. Raman and FTIR spectroscopy analyses provided further confirmation of the presence of CaO-NPs. Finally, DLS measurements revealed an average hydrodynamic diameter of 54.85 nm for the CaO-NPs, classifying them as macroporous. The macroporous structure suggests potential photocatalytic properties for the synthesized CaO-NPs.*

Keywords: *Nanoparticles, calcium-based, production, animal shells, properties*.

Richard Alexis Ukpe
Department of Chemistry, Federal University, Otuoke, Bayelsa State, Nigeria
Email: ukpera@fuotuoke.edu.ng
Orcid id: 0000-0002-1010-4433

1.0 Introduction

The most beneficial aspect of environmental science Is the identification of environmental problems and the design of solutions to prevent, control or solve the problem. In recent times, landfills have been overburdened by excessive waste generation, high cost of transportation, site contamination, health challenges and other consequences (Eddy *et al*., 2024a). Burning has become one of the operational options but considering solid waste, the energy required may be expensive and the by-product could be much more hazardous than the original waste. Consequently, current best practices in solid waste management are centred on the three cardinal points of recovery, reuse and recycling. Some studies have been reported on the conversion of several classes of solid waste to useful materials. For example, the synthesis of silicon nanoparticles from plant waste (Siddiqua *et al*., 2022), conversion of abattoir wastes to animal feed (Adebisi, *et al*., 2021), waste conversion to biofuel (Akin *et al*., 2023) and other reported cases. The shells of some animals are one class of solid wastes that have witnessed some levels of innovation in their management based on their chemical composition, extremely low cost of acquisition and environmental friendliness of the processed product. For example most of them are known for their role in serving as uque precursor for the production of CaO, $CaCO_3$ and $Ca(OH)_2$ nanoparticles . In our research group, processing of several types of crustacean shells to nanoparticles have been reported including some species of oyster (Eddy *et al*., 2023a-b, 2024b-c; Kelle *et al*.,2023; Odoemelam and Eddy, 2009; Ogoko *et al*. , 2023), periwinkle (Eddy *et al*., 2023c,2024b). Others have reported egg shells (Ismael *et al*., 2023; Nayar *et al*., 2021), snail shell (Ahmed *et al*., 2022), crab shells (Odiongenyi, 2022), scotch bonnet

(Odiongenyi, 2023) etc. Most of the reported works have shown that the quality of calcium oxide nanoparticles (CaONPs) obtained are preferred for various applications compared to the chemically obtained counterparts (Garg *et al*., 2024a-c). In this study, the mandate of our sponsored research is to report some works done on the synthesis of CaONPs from crab shell.

2.0 Materials and Methods

2.1 Synthesis of CaO-NPs

Oyster shells were collected as waste materials from the Oron fishing zone in Nigeria. The shells were washed severally with hot water to remove surface contaminants. The washed samples were dried to constant weight in an oven at 100 °C before reducing them to a powdered form using an electric motor-powered crusher. The $CaCO_3$-rich powder obtained from the shells was reacted with 2 M HCl and the resulting system was stirred continuously to remove CO_2 gas. The product of the reaction was hydrolysed with 50% NaOH solution to form $Ca(OH)_2$. When the reaction was complete, distilled water was used to wash off NaCl while the formed $Ca(OH)_2$ was dried to constant weight and finally calcined in a muffle furnace at 850 °C to produce CaONPs. Scheme 1 presents detailed steps employed for the synthesis of the CaO-NPs.

2.2 Characterization of CaO-NPs

The crystal profile of the CaONPs was evaluated using an X-ray diffraction (XRD) machine. The settings of the XRD machine were, k-alpha 1 = 1.5400 Å, k-beta = 1.39225 Å. The diffractometer type was fixed at 0000000011078671 while the generator was fixed at 40 mA, 45 kV. The system refractometer type was EMPYREAN. The diffractogram produced was obtained as a plot of intensity against 2[Theta]. In addition to the diffraction angles, other information such as density, the volume of the cell, d-spacing and Miller parameters were also obtained from the machine's output.. A UV-visible spectrophotometer was also used to detect the wavelength of maximum absorption by the CaO-NPs (i.e, λ_{max}). This was achieved by scanning the sample through a wavelength range of 200 to 1000 nm.

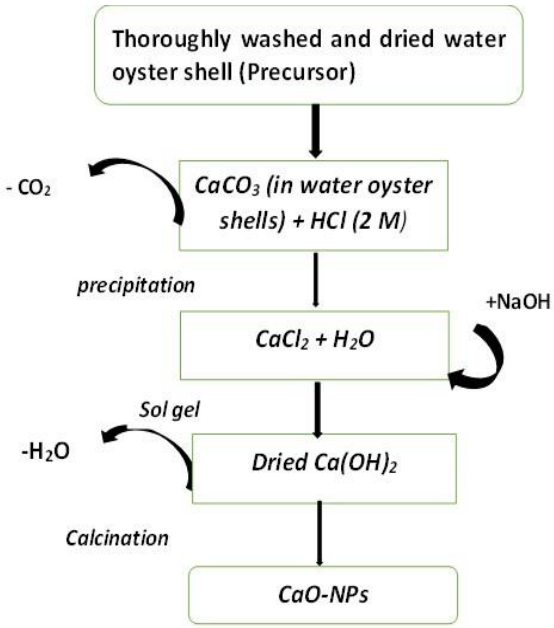

Scheme. 1: Scheme for the synthesis of CaONPs

4.0 Results and Discussion

4.1 Characterization of the CaO-NPs from Oyster Shell

The XRD profile of the synthesized CaO-NPs is shown in Fig. 1a. The diffractogram reveals the most prominent peak at 2θ = 29.40°. This peak value is in the range of values that have been confirmed to be typical for CaONPs, such as a maximum peak value of 2θ = 34° reported by Habte (2019) for CaO nanoparticles synthesized from waste eggshells using the sol-gel method. Toamahand Fadhil (2019) reported 2θ = 30 ° for calcium nanoparticles that were synthesized when $CaCl_2$ was used as a precursor while Butt, *et al*. (2015) reported 2θ

= 30 °. However, higher values such as 2θ = 30 (Alavi and Morsali, 2010), 32.2(Mohadi, *et al.*, 2018) and 37 °Khine*et al*. (2022) have also been reported for calcium oxide nanoparticles. Other peaks observed in the diffractogram were found at positions shown in Table 1. The fullwidth half maximum (FWHM) values for the respective position are also recorded in Table 1. Scherer's equation (equation 2) can be used to calculate the crystal size (D_{cryst}) of the synthesized CaONPs by substituting the values of FWHM at various angles of diffraction into the following equation (Canchanya-Huaman*et al*., 2021)

$$D_{cryst} = \frac{k\lambda}{(FWHM)cos\theta} \quad (2)$$

where λ is the wavelength of the Cu-K line excitation ($\lambda = 1.5406\, nm$) and k is the Scherer's constant, which is numerically equal to 0.9. Evaluated values of D_{cryst} for the various 2[theta] values are also recorded in Table 1. Based on the results, the average crystalline size of the nanoparticle is 57.18 nm. The distances between planes of atoms in CaO-NPs that gave rise to diffraction were also calculated using equation 3

$$\frac{1}{d^2} = \frac{h^2}{a^2} + \frac{k^2}{b^2} + \frac{l^2}{c^2} \quad (3)$$

where $h, k\ and\ l$ are the Muller indices while a, b and c are the sizes of the cube, which are equal to each other, hence $a = b = c$ and equation 3 becomes 4, while crystal plane spacing ($d_{(hkl)}$) can be evaluated through the application of equation 5 while the d-spacing was calculated using Bragg's equation (equation 6), which is simplified to equation 7

$$\frac{1}{d^2} = \frac{h^2 + k^2 + l^2}{a^2} \quad (4)$$

$$d_{(hkl)} = \sqrt{\frac{a^2}{h^2 + k^2 + l^2}} \quad (5)$$

$$n\lambda = 2dsin\theta \quad (6)$$

$$d = \frac{n\lambda}{2sin\theta}\ (n = 1) \quad (7)$$

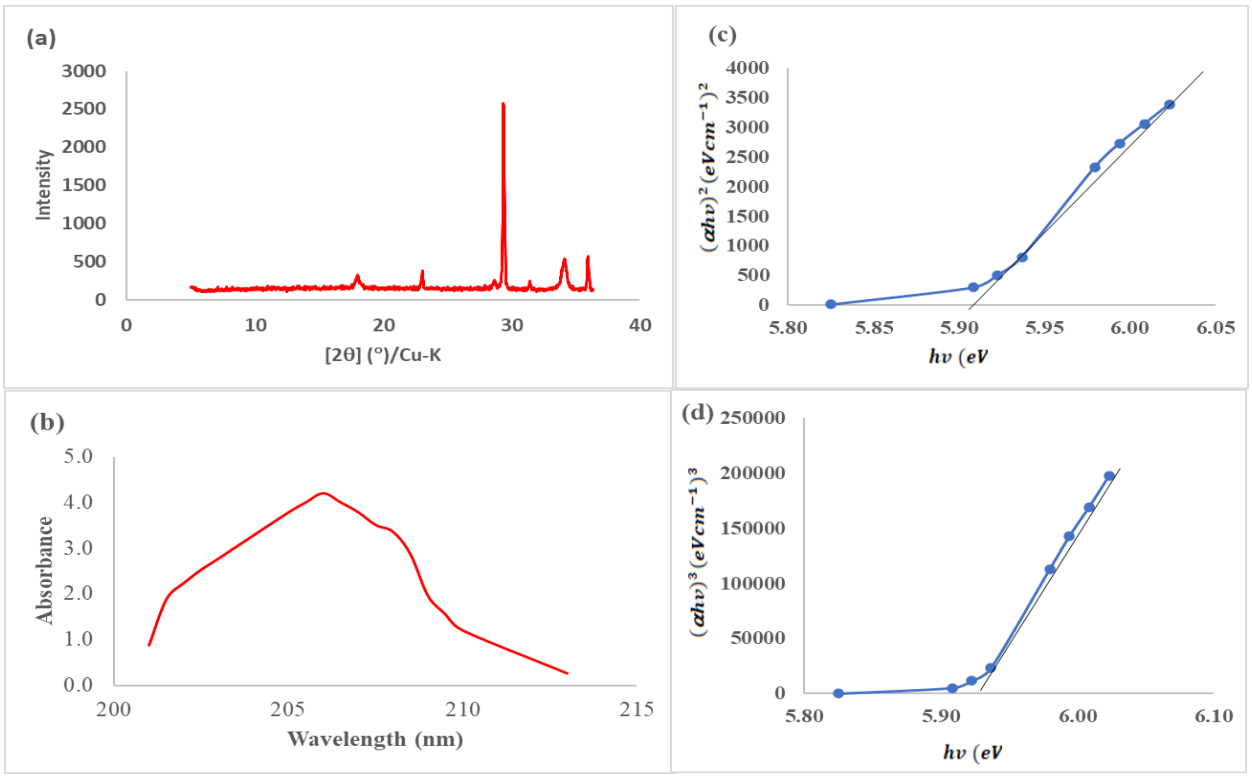

Fig. 1: (a) XRD diffractogram of CaO-NPs (b) UV absorption spectrum of CaO-NPs (c) Tauc's plot for direct allowed transition (d) Tauc's plot for indirect forbidden transition

Table 1: XRD parameters for the characterized CaO-NPs

2θ (*Radians*)	*FWHM* (*Radians*)	d (Å)	D_{cryst} (nm)	$d_{(hkl)}$(Å)
0.3141	0.0054	1.46	27.21	2.23
0.4024	0.0018	1.15	84.40	1.21
0.5008	0.0036	0.94	44.24	0.83
0.5130	0.0022	0.92	71.29	3.53
0.5486	0.0054	0.86	30.33	1.50
0.5961	0.0036	0.80	46.90	1.76

Parameters including a, h, l and k obtained from the XRD profile of the CaONPs were used to evaluate the d values for the various diffraction angles and the results obtained are also presented in Table 1. Calculating d-spacing ranged from 1.21 to 3.53 Å , which is comparable to a range of 1.388 to 3.015 Å reported for CaO nanoparticles synthesized using plant extract (Jadhav *et al*., 2022).

Other crystal indices evaluated from the XRD profile of the CaO-NPs were density (2.71 g/cm^3), cell volume ($3.6807 \times 10^{-4} pm^3$) and Bravais lattice parameters $\left(a = b = c = 4.9910\ \text{Å}, \propto = \beta = \gamma = 90^\circ\right)$

The UV visible spectrum of the synthesized CaO-NPs is shown in Fig. 1b. The spectrum reveals that the synthesized CaO-NPs absorb at 206 nm, which implies that the nanoparticles are absorbed in the UV region of the spectrum. The reported $\lambda_{max} = 206\ nm$ is not at variance with a $\lambda_{max} = 205\ nm$ reported by Aboutaleb and Mohammad (2013) for CaO-NPs synthesized by the reverse microemulsion techniques. One of the significant parameters that can be deduced from the UV absorption spectra of the synthesized CaO-NPs is the band gap, which was evaluated using the Planck equation as follows

$$E_{BG} = hv = \frac{hc}{\lambda_{max}} \qquad (8)$$

The substitution of Planck's constant (h = $6.626 \times 10^{-34} J/s$), speed of light ($(c = 3.00 \times 10^8 m/s$) and $\lambda_{max} = 206 \times 10^{-9} m$ into equation 8 gives the bandgap value of $9.4951 \times 10^{-19}\ J = 5.898\ eV$. The Tauc plot was also used to determine the bandgap and the transition type expected for the creation of holes and electrons in the CaO-NP. The primary form of the Tauc equation is given as follows (Hussein *et al*., 2020)

$$(\alpha hv)^{\sigma} = k_{Tauc}(hv - E_{BG}) \qquad (9)$$

where α is the absorption coefficient, h is the Planck constant, $v = hc/\lambda$),k_{Tauc} is the Tauc constant, σ is a factor that represents the nature of transition ($\sigma = 2, \frac{1}{2}, \frac{2}{3} or\ 3$ for direct, indirect, forbidden direct and forbidden indirect transition. Tauc's plots were developed for all possible transitions by plotting values of $(\alpha hv)^{\sigma}$ versus hv (for $\sigma = 2, \frac{1}{2}, \frac{2}{3}\ and\ 3\ respectively$. Bestfitness was obtained for $\sigma = 2\ and\ 3$ as shown in Fig. 1c and d respectively. Consequently, the direct allowed and indirect forbidden transitions are possible for the synthesized CaO-NP. The bandgaps evaluated through extrapolation for the direct allowed and indirect forbidden transitions were 5.90 and 5.93 eV respectively. Generally, the forbidden transition is not consistent with the prevailing selection rule. It is expected that until the photon energy exceeds 5.93 eV, the direct transition will dominate the spectral system of CaO-NP. The E_{BG} values evaluated from the Tauc plots are comparable to

the value evaluated from the Planck equation (i.e using equation 8).

The Raman spectrum of the CaO nanoparticles is shown in Fig. 2a. The spectrum reveals a major peak at 2450 nm and minor peaks at 700, 763 and 1221 nm. Literature is scanty on the establishment of reference Raman bands for CaO nanoparticles. However, some studies have been conducted on the Raman spectra of CaO such as the observation of. Raman scattering bands of CaO around 655, 780, 1078 and 1106 cm^{-1} by Capriotti and Quaini(2012). Consequently, the band they observed at 655 cm^{-1} which can be compared with the band at 696 cm^{-1} obtained for CaO nanoparticles in this work was regarded as the reference peak. Also, the band at 780 cm^{-1} for CaO can be compared to the band at 756 cm^{-1} obtained in this study and is attributed to the optical transversal and longitudinal band. However, Rincon-Yoya*et al*. (2016) observed major peaks at 1018 and 1086 cm^{-1} for CaO that were synthesized from two different methods. Raman shift was observed to be a function of particle size, indicating that as the particle size decreases, the wavelength also increases. Therefore, the peaks at 108 and 1218 cm^{-1} observed in the present work are attributed CaO nanoparticles (CaO-NP), whose size dimension is far lower than that of CaO, and hence the expected incremental Raman shift.

The FTIR spectrum of the synthesized CaO-NP shown in Fig. 2breveals three peaks including fingerprint peaks at 712 and 872 cm^{-1} (Habe, 2019). Also, a prominent peak was observed at 338 cm^{-1}. Although Sing *et al*. (2016) have reported such a peak (at 338 cm^{-1}) as unique but not fully understood, the remark made by Zyiagina*et al.* (2022) after theobservation of a similar peak, constitutes strong evidence as a representative peak for CaO nanoparticles.

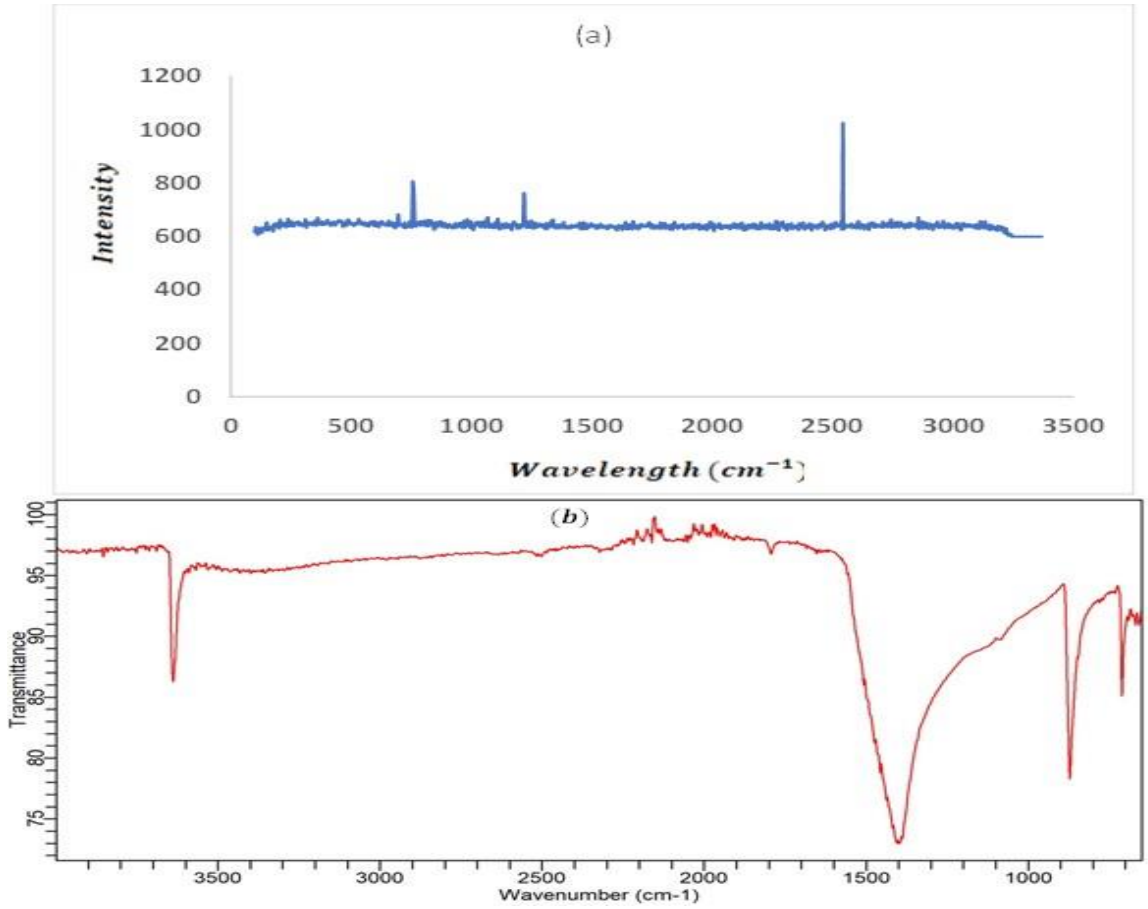

Fig. 2: (a) Raman (b) FTIR spectrum of CaO-NP

The dynamic light scattering (DLS) measurement was implemented to determine the average diameter of the CaO-NP. Fig. 3 shows distribution plots based on the variation of particle size with the number, volume and intensity respectively. Generally, the DLS method measures the hydrodynamic diameter, which is based on the Stokes law (equation 10)

$$d_{(H)} = \frac{k_B T}{3\pi\eta D_{diffus}} \qquad (10)$$

where $d_{(H)}$ is the hydrodynamic diameter, k_B is the Boltzmann constant, T is the temperature, η is the viscosity of the dispersant and D_{diffus} is the diffusion coefficient of the medium.

The presented peaks (Fig.3) reveal three major peaks based on the number, volume and intensity. The distribution based on the number of particles is more evenly spread, followed by the distribution based on the volume and lastly by the distribution based on the intensity. This is because the volume of a sphere measured by the DLS machine is $\frac{4}{3}\pi \times \left(\frac{d}{2}\right)^3$ and the intensity is proportional to the sixth root of the diameter $(i.e, intensity \propto d^6)$. The corresponding diameters for the peaks are also shown in the figure while the average Z-average, which is the best approximation for the diameter of the particle was 54.85 nm.

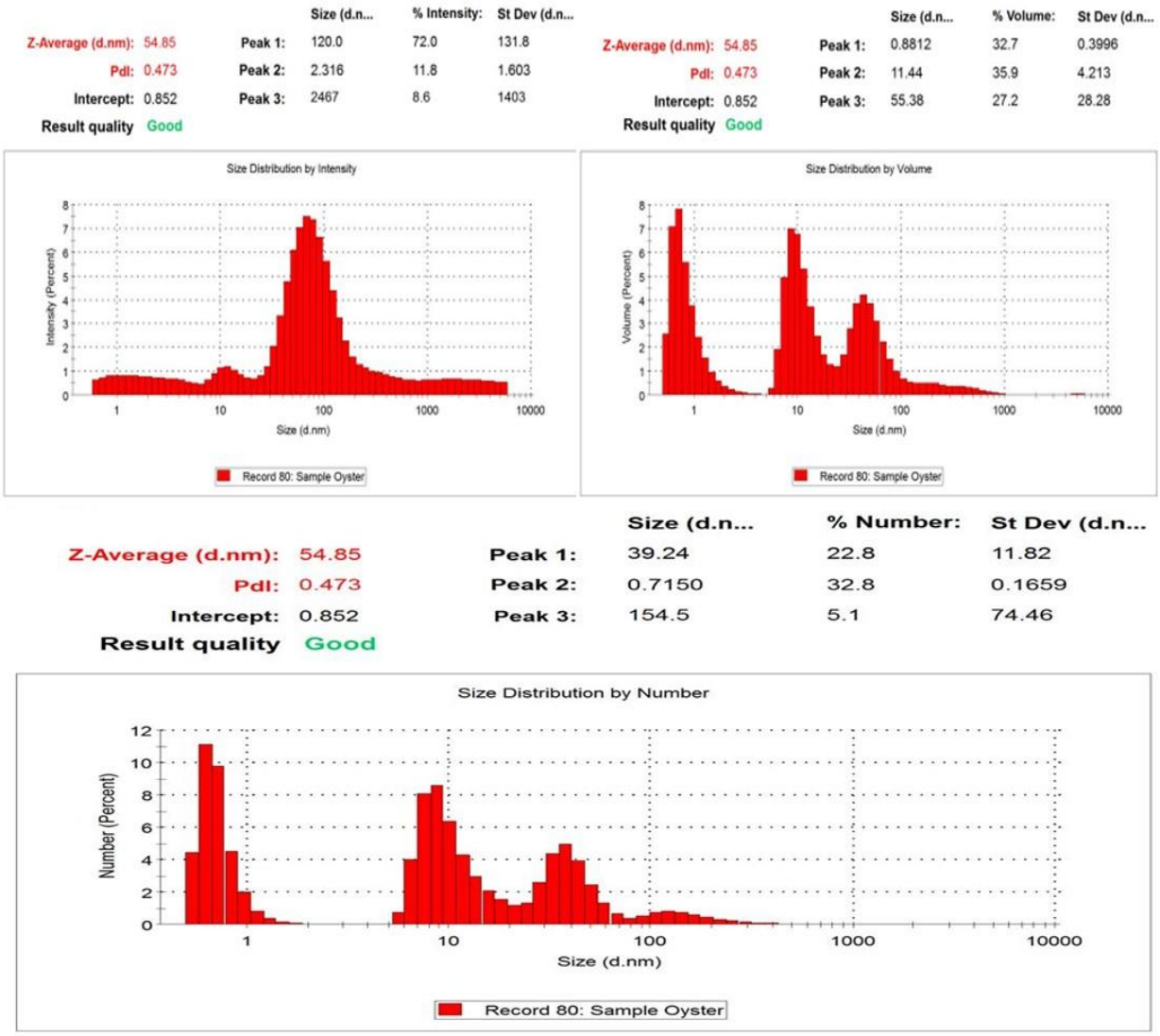

Fig. 3: DLS distribution profiles for the CaONPs

The Z-Average (d.nm) value, displayed at the top left corner of each plot, represents the average hydrodynamic diameter of the particles as measured by DLS. In this case, the Z-average while the diameter is 54.85 nm as stated before. Each plot has multiple peaks, labelled Peak 1, Peak 2, etc. These peaks represent populations of particles with similar sizes. The x-value (e.g., 120.0 nm for Peak 1 in the Intensity plot) indicates the size around which the particles in that population are clustered. Therefore, the ratio of pore volume to the total volume of the synthesized CaONPs (which defines its porosity) best fits the macroporous class of nanoparticles because its particle size is slightly greater than 50 nm (Eddy *et al*., 2022; Lan and Zhao, 2022). Somo *et al*. (2022) identified macroporous class as materials with unique optical-related photonic bandgaps as well as optical stopped bands. Therefore, the synthesized CaO-NP will likely exhibit a good photocatalytic tendency.

4.0 Conclusion

This study successfully synthesized calcium oxide nanoparticles (CaO-NPs) from oyster shells, a waste material. The characterization techniques employed (XRD, UV-visible spectroscopy, Raman spectroscopy, FTIR spectroscopy, and DLS) confirmed the formation of CaO-NPs with an average crystal size of 57.18 nm and a macroporous structure with an average hydrodynamic diameter of 54.85 nm. The UV-visible spectrum indicated absorption in the ultraviolet region, and the band gap energy was calculated to be around 5.9 eV.

This research demonstrates the feasibility of extracting valuable nanomaterials, CaO-NPs in this case, from oyster shells, a waste product. The characterization results confirm the successful synthesis of CaO-NPs with properties potentially suitable for photocatalysis due to their macroporous structure and band gap energy.

Given the promising characteristics of the synthesized CaO-NPs, further research is recommended to explore their photocatalytic activity. This could involve investigating their ability to degrade pollutants or generate clean energy under light irradiation. Additionally, research could optimize the synthesis process to control the size, morphology, and surface area of the CaO-NPs for enhanced photocatalytic performance. Finally, exploring the potential of using waste crab shells for similar nanoparticle synthesis could broaden the applicability of this waste valorization approach.

5.0 References

Aboutaleb, G. J. G. & Mohammad, I. (2013). Characterization of $CaCO_3$ Nanoparticles synthesized by reverse microemulsion technique in different concentrations of surfactants. *Iranian Journal of Chemistry and Chemical Engineering*, 32, 3, pp. 27-35.

Adebisi, J. A., Agunsoye, J. O., Ahmed, I. I., Bello, S. A., Haris, M., Ramakokovhu, M. M., & Hassan, S. B. (2021). Production of silicon nanoparticles from selected agricultural wastes. *Materials Today: Proceedings*, 38, 2, pp. 669-674. https://doi.org/10.1016/j.matpr.2020.03.658.

Ahmed, H. Y., Safwat, N., Shehata, R., Althubaiti, E. H., Kareem, S., Atef, A., Qari, S. H., Aljahani, A. H., Al-Meshal, A. S., Youssef, M., et al. (2022). Synthesis of natural nano-hydroxyapatite from snail shells and its biological activity: Antimicrobial, antibiofilm, and biocompatibility. *Membranes*, 12, 408. https://doi.org/10.3390/membranes12040408.

Akın, M., Bartkiene, E., Özogul, F., Eyduran, S. P., Trif, M., Lorenzo, J. M., & Rocha, J. M. (2023). Conversion of organic wastes into biofuel by microorganisms: A bibliometric review. *Cleaner and Circular Bioeconomy*, 6, 100053.

https://doi.org/10.1016/j.clcb.2023.100053.

Alavi, M. A. & Morsali, A. (2010) Ultrasonic-assisted synthesis of Ca(OH)2 and CaO nanostructures, Journal of Experimental Nanoscience, 5, 2, pp. 93-105, DOI: 10.1080/1745808090330561.

Butt, A. R., Ejaz, S., Baron, J. C., Ikram, M. & Ali, S. (2015). CaO nanoparticles as a potential drug delivery agent for biomedical application. *Digest Journal of Nanomaterials and Biostructures*, 10, 3, pp. 799 – 809.

Canchanya-Huaman, Y., Mayta-Armas, A. F., Pomalaya-Velasco, J., Bendezú-Roca, Y., Guerra, J. A. & Ramos-Guivar, J. A. (2021). Strain and Grain Size Determination of CeO_2 and TiO_2 Nanoparticles: Comparing Integral Breadth Methods versus Rietveld, μ-Raman, and TEM. Nanomaterials (Basel). 11, 9, 2311. doi: 10.3390/nano11092311.

Capriotti, L. & Quaini, A. (2012). *High temperature behaviour of nuclear materials investigated by laser heating and fast pyrometry*. M.Sc Thesis, doi.10.13140/RG.2.1.1969.0967.

Chaibakhsh, N., Ahmadi, N. & Zanjanchi, M. A. (2016). Optimization of photocatalytic degradation of neutral red dye using TiO_2 nanocatalyst via Box-Behnken design, *Desalination and Water Treatment*, 57, 20, pp. 9296-9306 , doi: 10.1080/19443994.2015.1030705.

Eddy, N. O., Garg, R., Garg, R., Aikoye, A. & Ita, B. I. (2022). Waste to resource recovery: mesoporous adsorbent from orange peel for the removal of trypan blue dye from aqueous solution. *Biomass Conversion and Biorefinery*, doi: 10.1007/s13399-022-02571-5.

Eddy, N. O., Garg, R., Garg, R., Eze, S. I., Ogoko, E. C., Kelle, H. I., Ukpe, R. A., Ogbodo, R. & Chijoke, F. (2023). Sol-gel synthesis, computational chemistry, and applications of CaO nanoparticles for the remediation of methyl orange contaminated water. *Advances in Nano Research*, https://doi.org/10.12989/anr.2023.15.1.000

Eddy, N. O., Garg, R., Ukpe, R. A., Akpanudo, N. W., Abugu, H., Garg, R., Anjum, A. & Anand, B. (2024a). *Chapter 10; Ethical issues Ethical and environmental implication associated with the application of nanoparticles*. doi:: 10.4018/979-8-3693-1094-6.ch010. Book Chapter Published by IGI, USA. pp. 274-299.

Eddy, N. O., Garg, R., Ukpe, R. A., Ameh, P. O., Gar, R., Musa, R., , Kwanchi, D., Wabaidur, S. M., Afta, S., Ogbodo, R., Aikoye, A. O. & Siddiqu, M. (2024c). Application of periwinkle shell for the synthesis of calcium oxide nanoparticles and in the remediation of Pb^{2+}-contaminated water. *Biomass Conversion and Biorefinery*, DOI: 10.1007/s13399-024-05285-y.

Eddy, N. O., Jibrin, J. I., Ukpe, R. A., Odiongenyi, A. O., Kasiemobi, A. M., Oladele, J. O. & Runde, M. (2024b). Experimental and Theoretical Investigations of photolytic and photocatalysed degradations of crystal violet dye (CVD) in Water by oyster shells derived CaO nanoparticles (CaO-NP), *Journal of Hazardous Materials Advances*, 100413, https://doi.org/10.1016/j.hazadv.2024.100413.

Eddy, N. O., Odiongenyi, A. O., Garg, R., Ukpe, R. A., Garg, R., El Nemir, A., Ngwu, C. M. & Okop, I. J. (2023a). Quantum and experimental investigation of the application of *Crassostrea gasar* (mangrove oyster) shell–based CaO nanoparticles as adsorbent and photocatalyst for the removal of procaine penicillin from aqueous solution. *Environmental Science and Pollution*

Research, doi:10.1007/s11356-023-26868-8.

Eddy, N. O., Ukpe, R. A., Ameh, P., Ogbodo, R., Garg, R. & Garg, R. (2023b). Theoretical and experimental studies on photocatalytic removal of methylene blue (MetB) from aqueous solution using oyster shell synthesized CaO nanoparticles (CaONP-O). *Environmental Science and Pollution Research*, https://doi.org/10.1007/s11356-022-22747-w.

Garg, R., Garg, R. & Eddy, N. O. (2024a). Chapter 2: *Application of nanocoating smart and sustainable protection.* doi: 10.4018/979-8-3693-3136-1.ch002, Book Chapter Published by IGI, USA. pp. 28-56**.**

Garg, R., Garg, R. & Eddy, N. O**.** (2024b). Chapter 4: Applications of nocomposites in Water Remediation: A Mechanistic Overview, doi: 10.4018/979-8-3693-1094-6.ch004. Pp. 102-120.

Garg, R., Mittal, M., Tripathi, S. & Eddy, N. O. (2024c). Core to concept: synthesis, structure, and reactivity of nanoscale zero-valent iron (NZVI) for wastewater remediation. *Environmental Science and Pollution Research*. Advance online publication. https://doi.org/10.1007/s11356-024-33197-x

Habe, L. (2019). Synthesis of nano-calcium oxide from waste eggshell by sol-gel method. sustainability, 11, 11, doi: 10.3390/su11113196.

Hussein, A. M., Dannoun, E. M. A., Aziz, S. B., Brza, M. A., Abdulwahid, R. T., Hussen, S. A., Rostam, S., Mustafa, D. M. T. & Muhammad , D. S. (2020). Steps toward the band gap identification in polystyrene based solid polymer nanocomposites integrated with tin titanate nanoparticles. *Polymers (Basel).* 2020 Oct 10;12(10):2320. doi: 10.3390/polym12102320.

Ismael, E., Fahim, K. M., Ghorab, S. M., Hamouda, R. H. ., Rady, A. M., Zaki, M. M., & Gamal, A. M. . (2023). Sustainable recycling of poultry eggshell waste for the synthesis of calcium oxide nanoparticles and evaluating its antibacterial potency against food-borne pathogens. *Journal of Advanced Veterinary Research*, 14, 1, pp. 130-134.

Jadhav, V., Bhagare, A., Wahab, S., Lokhande, D., Vaidya, C., Dhayagude, A., Khalid, M., Aher, J., Mazni, A. & Dutta, M. (2022). Green synthesized calcium oxide nanoparticles (CaO NPs) using leaves aqueous extract of *Moringa oleifere*and evaluation of their antibacterialsactivities. *Journal of Nanomaterials*, https://doi.org/10.1155/2022/9047507.

Kelle, H. I., Ogoko, E. C., Akintola O & Eddy, N. O. (2023). Quantum and experimental studies on the adsorption efficiency of oyster shell–based CaO nanoparticles (CaONPO) towards the removal of methylene blue dye (MBD) from aqueous solution. Journal: Biomass Conversion and Biorefinery, DOI : 10.1007/s13399-023-04947-7.

Khine, E.E., Koncz-Horvath, D., Kristaly, F., Ferenczi, T., Karacs, G., Baumli, P and Kaplay, G. (2022). Synthesis & characterization of calcium oxide nanoparticles for CO_2 capture. *J Nanopart Res*, 24, 139 (2022). https://doi.org/10.1007/s11051-022-05518-z

Lan, K. & Zhao, D. (2022). Functional ordered mesoporous materials : Present and future. Nano Letters, 22 (8): 3177-3179, doi.org/10.1021/acs.nanolett.2c00902.

Akın, M., Bartkiene, E., Özogul, F., Eyduran, F. P., Trif, M., Lorenzo, J. M. & Rocha, J. M. (2023). Conversion of organic wastes into biofuel by microorganisms: A bibliometric review. *Cleaner and Circular*

Bioeconomy, 6, 100053. ISSN 2772-8013. https://doi.org/10.1016/j.clcb.2023.100053.

Mohadi, R., Sueb, A., Anggraini, K. & Lesbani, A. (2018). Calcium Oxide Catalyst Based on Quail Eggshell for Biodiesel Synthesis from Waste Palm Oil. *J. Pure App. Chem. Res*., 2018, 7(2), 130-139, DOI: 10.21776/ub.jpacr.2018.007.02.390.

Nayar, R., Waghmare, S., Nageshwar, P., Najar, M., Singh, U., & Agnihotri, A. (2021). Preparation of calcium oxide nanoparticles from industry rejects: Recovery and value addition of mineral values. *Materials Today: Proceedings, 39, 4, pp.* 1722-1726. https://doi.org/10.1016/j.matpr.2020.06.300

Odiongenyi, A. O. (2022). Influence of sol gel conversion on the adsorption capacity of crab shell for the removal of crystal violet from aqueous solution. *Communication in Physical Sciences*, 8, 1, pp. 121-127.

Odiongenyi, A. O. (2023). Adsorption efficiency of scotch bonnet shells as a precursor for calcium oxide nanoparticles and an adsorbent for the removal of amoxicillin from aqueous solution. *Communication in Physical Sciences*, 9, 3, pp. 367-382.

Odoemelam, S. A. & Eddy, N. O. (2009). Studies on the use of oyster, snail and periwinkle shells as adsorbents for the removal of Pb^{2+} from aqueous solution. *E. Journal of Chemistry* 6, 1, pp. 213-222.

Ogoko, E. C., Kelle, H. I., Akintola, O. & Eddy, N. O. (2023). Experimental and theoretical investigation of *Crassostrea* gigas (gigas) shells based CaO nanoparticles as a photocatalyst for the degradation of bromocresol green dye (BCGD) in an aqueous solution. *Biomass Conversion and Biorefinery*. https://doi.org/10.1007/s13399-023-03742-8.

Rincon-Yoya, M., Raba, A. M. & Barba-Ortega, J. J. (2016). Synthesis of calcium oxide by means of two different chemical processes. *Universidad, Ciencia y Tecnología*, 20, 81, pp. 188-192.

Siddiqua, A., Hahladakis, J. N., & Al-Attiya, W. A. K. A. (2022). An overview of the environmental pollution and health effects associated with waste landfilling and open dumping. *Environmental Science and Pollution Research*, 29, pp. . 8514–58536. https://doi.org/10.1007/s11356-022-21578-z

Singh, B., Fang, Y. & Johnson, C. T. A Fourier-Transform Infrared Study of biochar aging in soils. Soil Sci Soc Am J., 80, 3, pp. 613-622. doi: 10.2136/sssaj2015.11.0414.

Somo, T., Hato, M. J., & Modibane, K. D. (2022). Characterization of Macroporous Materials. In A. Uthaman, S. Thomas, T. Li, & H. Maria (Eds.), *Advanced Functional Porous Materials*, pp. 100-120). DOI: 10.1007/978-3-030-85397-6_4.

Toamah, W. O. and Fadhil, K. (2019). Preparation of nanoparticles from CaO and use it for removal of chromium (II), and mercury (II) from aqueous solutions. The 1st International Scientific Conference on Pure Science IOP Conf. Series: *Journal of Physics: Conf. Series* 1234, doi:10.1088/1742-6596/1234/1/012086.

Uthaman, A., Thomas, S., Li, T. & Maria, H. (eds) Advanced Functional Porous Materials. Engineering Materials. Springer, Cham. doi.org/10.1007/978-3-030-85397-6_4.

Zyiagina, B. B., Drits, V. A. & Dorzhieva, O. V. (2020). Distinguishing features and identification criteria for k-dioctahedral 1*m* micas (illite-aluminoceladonite and illite-glauconite-celadonite series) from middle-infrared spectroscopy data. *Minerals*, *10*(2),

153; https://doi.org/10.3390/min10020153.

Compliance with Ethical Standards Declarations

The authors declare that they have no conflict of interest.

Data availability

All data used in this study will be readily available to the public.

Consent for publication

Not Applicable

Availability of data and materials

The publisher has the right to make the data Public.

Competing interests

The authors declared no conflict of interest.

Funding

The work was funded by the Tertiary Education Trust Fund (NRF) through Prof. Nnabuk Okon Eddy as the principal Investigator (Grant No: TETF/ES/DR&D-CE/NRF2020/SET1/98/VOL.1).